Proceedings of Global Power and Propulsion Society
ISSN-Nr: 2504-4400
GPPS Chania20
7th – 9th September, 2020
www.gpps.global

# GPPS-CH-2020-0053

# THE EFFECT OF ROUGH-WALL BOUNDARY CONDITIONS ON RANS-BASED TRANSITION PREDICTION

**Robert Alldieck**
**Formerly**
**Institute of Turbomachinery and Fluid Dynamics**
**Leibniz Universität Hannover**
Garbsen, 30823, Germany

**Hendrik Seehausen** *
**Institute of Turbomachinery and Fluid Dynamics**
**Leibniz Universität Hannover**
seehausen@tfd.uni-hannover.de
Garbsen, 30823, Germany

**Florian Herbst**
**Formerly**
**Institute of Turbomachinery and Fluid Dynamics**
**Leibniz Universität Hannover**
Garbsen, 30823, Germany

**Joerg R. Seume**
**Institute of Turbomachinery and Fluid Dynamics**
**Leibniz Universität Hannover**
Garbsen, 30823, Germany

## ABSTRACT

*A study on the prediction of transition-based Reynolds-Averaged Navier-Stokes (RANS)-equations of rough-wall boundary conditions is presented at various pressure gradients. This work focuses on the interaction of turbulence and transition models implemented in the flow solver TRACE in order to a rough-wall boundary condition. An annular wind tunnel test case is used to study the quality of transition prediction of the model combinations when simulating surface roughness under different pressure gradients. The numerical results are compared with experimental data generated with sand paper roughness. Subsequently, the interdependencies of the investigated model combinations are analyzed by focusing on the model equations. The results show that the transition process is already affected by rough walls, even if the transition model has no sensitivity to surface roughness implemented. Moreover, none of the model combinations can precisely predict the experimental results. As an outlook, ideas to further improve the modeling of the rough wall effect on the transition onset are described.*

## INTRODUCTION

In recent years, a substantial progress in transition modeling for turbomachinery applications has been made. Mayle (1991) emphasized the significance of laminar-turbulent transition in gas turbines and stated the different transition modes, i.e. natural and bypass-transition, separation-induced transition, and wake-induced transition. To account for the different modes of transition, different approaches for modeling the transition evolved in the past decades (Suzen et al., 2002; Menter et al., 2006; Kožulović, 2007; Stripf et al., 2008; Langtry and Menter, 2009; Menter et al., 2015). Most of the transition models are based on the correlations of Abu-Ghannam and Shaw (1980) and, thus, are designed to trigger the turbulence model and not to predict the physical effect in detail (Langtry and Menter, 2009). In contrast, laminar kinetic energy models present a more physically-based approach for transition modeling (Walters and Leylek, 2004; Walters and Cokljat, 2008). However, to achieve an increase in gas turbine efficiency and consequently a more accurate prediction of deterioration-based performance losses, extensions of the transition models by second order effects, i.e. surface roughness, are needed (Boyle and Senyitko, 2003; Hohenstein et al., 2013a; Gilge et al., 2017). Extensions for other secondary flow effects, such as injection-induced transition or crossflow-induced transition, are proposed by Herbst et al. (2014) and Müller and Herbst (2014). Several approaches exist for the turbulence models to incorporate second-order flow effects. Wilcox (1988) adjusts the dissipation rate $\omega$ at the wall depending on the surface roughness. This is not suitable for surface structures such as riblets due to their drag-decreasing effects. Thus, Koepplin et al. (2017) applied a damping function to the destruction term of the dissipation rate $\omega$.

*Address all correspondence to this author.

As described by Schlichting (1936) and Feindt (1956), surface roughness (compared to a smooth surface) generally moves the laminar-turbulent transition upstream and increases the turbulent fluctuations in the turbulent boundary layer. At high Reynolds number with an almost turbulent boundary layer for a hydraulically smooth surface, Hummel et al. (2005) found that the total pressure loss of turbine blades is increased up to 40% by surface roughness. In contrast, at low Reynolds numbers, surface roughness can lower the aerodynamic losses by eliminating a laminar separation (Boyle and Senyitko, 2003). A correct prediction of the roughness-induced transition is also important for the heat transfer design of turbine blades which show an increase in heat transfer coefficients by up to 50% in the turbulent boundary layer caused by surface roughness (Stripf et al., 2005). Bons (2010) presents a detailed overview of the effect of surface roughness in gas turbines.

Based on the different use cases, i.e. prediction of heat transfer or aerodynamic losses, different approaches considering surface roughness in transition modeling have been developed (Stripf et al., 2008; Dassler, 2013). In this paper, the prediction quality of the effect of surface roughness on skin friction and velocity profile will be analyzed. Most of the correlations for modeling the skin friction across rough surfaces are correlated with the equivalent sand-grain roughness $k_s$, in both laminar and turbulent boundary layers (Bons, 2010; Dassler, 2013; Wilcox, 1988). The equivalent sand-grain roughness $k_s$ assumes that the effect of each technical roughness can be equally achieved by a uniform layer of sand-grains with a diameter $k_s$ with an equivalent effect based on skin friction losses (Nikuradse, 1933; Schlichting, 1936). To model the effect of surface roughness in the transition model, Dassler (2013) used the transition model formulation of Langtry and Menter (2009) and added a third transport equation. The third transport equation allows transporting the flow disturbances induced by the surface roughness into the complete flow field via the variable $A_r$. However, Hohenstein et al. (2013b) and Alldieck (2019) show still existing deficits in transition modeling of rough surfaces, especially of complex surface structures.

So far, little attention has been paid to the interaction of transition and turbulence models considering a rough-wall boundary condition. Based on the transition model formulations, the authors assume that the interaction, in particular the effect of the rough-wall boundary condition of the turbulence model on the transition model, has a significant effect on the transition prediction. This leads to the question: which parameters of the turbulence model are used by the transition model, and how significant is the effect of each parameter on the roughness-induced transition? Answering this question is essential, when improving or extending existing models by second order transition modes due to surface roughness. To this end, this paper focuses on the interaction of existing transition and turbulence models implemented in the non-commercial flow solver TRACE considering rough-wall boundary condition. First, the prediction quality of the roughness transition model in combination with the $k$-$\omega$ turbulence model is validated with experiments conducted in an annular wind tunnel under different pressure gradients and a variation of surface roughness heights (Feindt, 1956). Secondly, the transition onset prediction of model combinations which do not feature a rough-wall boundary condition in transition modeling is studied.

## FUNDAMENTALS

This section describes the incorporation of the rough-wall boundary condition in the turbulence and transition models. First, the model formulations of the $k$-$\omega$ model (Wilcox, 1988) and SST model (Menter, 1994) implemented in the non-commercial flow solver TRACE are described. Secondly, the $\gamma$-$Re_\theta$ model (Langtry and Menter, 2009) and the roughness extension (Dassler et al., 2012; Dassler, 2013) are introduced.

### Turbulence Model

The turbulence models used in this study are based on the eddy viscosity $\mu_T$. In the $k$-$\omega$ turbulence model by Wilcox (1988), the eddy viscosity $\mu_T$

$$\mu_T = \frac{\rho k}{\omega} \tag{1}$$

is defined by the turbulent kinetic energy $k$

$$\frac{D(\rho k)}{Dt} = \overbrace{\tau_{ij}\frac{\partial u_i}{\partial x_j}}^{P} - \overbrace{\beta^*\rho\omega k}^{D} + \frac{\partial}{\partial x_j}\left[(\mu + \sigma_k\mu_T)\frac{\partial k}{\partial x_j}\right] \tag{2}$$

and the specific dissipation rate $\omega$:

$$\frac{D(\rho\omega)}{Dt} = \alpha\frac{\omega}{k}\tau_{ij}\frac{\partial u_i}{\partial x_j} - \beta\rho\omega^2 + \frac{\partial}{\partial x_j}\left[(\mu + \sigma_\omega\mu_T)\frac{\partial \omega}{\partial x_j}\right]. \tag{3}$$

The term $\tau_{ij}\frac{\partial u_i}{\partial x_j}$ describes the production of the turbulent kinetic energy and models the Reynolds stress tensor using the Boussinesq approximation

$$\tau_{ij} = -\rho\overline{u_i' u_j'} = 2\mu_T S_{ij}^* - \frac{2}{3}\rho k\delta_{ij} \tag{4}$$

with the trace-less mean strain-rate tensor $S_{ij}^*$. By contrast, Menter (1994) redefined the equation of the eddy viscosity in the SST turbulence model as follows

$$\mu_T = \frac{a_1\rho k}{\max(a_1\omega; |\Omega|F_2)} \tag{5}$$

with $a_1 = 0.31$ and the absolute value of the vorticity $|\Omega|$. The function $F_2$ is designed to be equal one in boundary layer flows and zero in the free stream. As reported by Menter (1994), this limitation implements the Bradshaw assumption that the shear stress $\tau_{ij}$ is proportional to the turbulent kinetic energy $k$. This

is essential in adverse pressure gradient boundary layers, where the conventional formulation overestimates the eddy viscosity $\mu_\mathrm{T}$ due to the high production of turbulent kinetic energy $k$. To eliminate the sensitivity to the free stream turbulence of the conventional $k$-$\omega$ formulation, the transport-equation for the specific dissipation rate $\omega$ is adapted by a cross-diffusion term outside the boundary layer:

$$\begin{aligned}\frac{D(\rho\omega)}{Dt} =& \alpha\frac{\omega}{k}\tau_{ij}\frac{\partial u_i}{\partial x_j} - \beta\rho\omega^2 + \frac{\partial}{\partial x_j}\left[(\mu+\sigma_\omega\mu_\mathrm{T})\frac{\partial\omega}{\partial x_j}\right] \\ &+ \underbrace{2(1-F_1)\rho\sigma_{\omega2}\frac{1}{\omega}\frac{\partial k}{\partial x_j}\frac{\partial\omega}{\partial x_j}}_{\text{cross-diffusion}}. \end{aligned} \tag{6}$$

In the near wall boundary layer, the blending factor $F_1$ disables the cross-diffusion term. Outside the boundary layer, the factor $F_1$ is designed to be equal to zero and, thus, activate the $k$-$\epsilon$ formulation. Besides switching between both turbulence model formulations, the blending factor $F_1$ is used to combine the constants $\phi_1$ and $\phi_2$ of both models:

$$\phi = F_1\phi_1 + (1-F_1)\phi_2. \tag{7}$$

However, in both turbulence models, the $k$-$\omega$ formulation is solved near the wall. This yields the advantage that the effect of surface roughness can be modeled by adapting the dissipation $\omega$ at the wall. Thus, Wilcox (1988) redefines the specific dissipation rate at the wall for rough surfaces as:

$$\omega_\mathrm{rough} = \frac{u_\tau^2}{\nu}S_R \quad \text{with} \quad u_\tau = \sqrt{\frac{\tau_\mathrm{W}}{\rho_\mathrm{W}}}. \tag{8}$$

The modification term $S_R$

$$S_R = \begin{cases}\left(\frac{50}{k_\mathrm{s}^+}\right)^2 & k_\mathrm{s}^+ < 25 \\ \frac{100}{k_\mathrm{s}^+} & k_\mathrm{s}^+ \geq 25\end{cases} \tag{9}$$

incorporates the effect of a rough wall and is correlated with the non-dimensional sand-grain roughness $k_\mathrm{s}^+$. This correlation reduces the specific dissipation $\omega$ at the wall for increasing surface roughness. A decrease of the specific dissipation $\omega$ results in an increase of the eddy viscosity $\mu_\mathrm{T}$ and turbulent kinetic energy $k$. Thus, higher turbulent fluctuations and viscous losses occur. Wilcox (1988) shows that the modification of the specific dissipation $\omega$ at the wall can accurately predict the velocity profile affected by a rough surface. Unfortunately, the eddy-viscosity limiter ensuring the Bradshaw assumption of the SST model disables the rough-wall condition of the $k$-$\omega$ formulation (Hellsten and Laine, 1997). Hellsten and Laine (1997) solved this problem by introducing an additional limiter which deactivates the Bradshaw assumption in specific regions such as, in the sublayer and roughness layer. However, the additional limiter is not implemented in TRACE and, thus, not used in this study.

## Transition Model

In contrast to the turbulence models, transition models rarely consider a rough-wall boundary condition. One reason is of course the difficulty in combining the different transition modes (Mayle, 1991). Thus, the first transition models were developed for first order effects, i.e. natural and bypass transition, separation-induced transition, and wake-induced transition. Consequently, no consideration of a rough-wall boundary condition is implemented in the original formulation of the $\gamma$-$Re_\theta$ model by Langtry and Menter (2009). The $\gamma$-$Re_\theta$ model is based on local variables of each cell without the need for any boundary layer integration. The transition process is modeled by two transport equations, i.e. one for the intermittency $\gamma$

$$\frac{D(\rho\gamma)}{Dt} = P_\gamma - E_\gamma + \frac{\partial}{\partial x_j}\left[\left(\mu+\frac{\mu_\mathrm{T}}{\sigma_f}\right)\frac{\partial\gamma}{\partial x_j}\right] \tag{10}$$

and one for the momentum thickness Reynolds number $\tilde{Re}_{\theta t}$:

$$\frac{D(\rho\tilde{Re}_{\theta t})}{Dt} = P_{\theta t} + \frac{\partial}{\partial x_j}\left[\sigma_{\theta t}(\mu+\mu_\mathrm{T})\frac{\partial\tilde{Re}_{\theta t}}{\partial x_j}\right]. \tag{11}$$

The production term $P_{\theta t}$

$$P_{\theta t} = c_{\theta t}\frac{\rho}{t}\left(Re_{\theta t} - \tilde{Re}_{\theta t}\right)(1-F_{\theta t}) \tag{12}$$

forces the transport variable $\tilde{Re}_{\theta t}$ to take the value of the local momentum thickness Reynolds number $Re_{\theta t}$ outside of the boundary layer. The local momentum thickness Reynolds number $Re_{\theta t}$ is correlated with the turbulence intensity Tu, pressure gradient parameter $\lambda_\theta$, and acceleration parameter $K$ described in Menter et al. (2006). Inside the boundary layer, the production term of $\tilde{Re}_{\theta t}$ is disabled by a blending factor $F_{\theta t}$. Thus, the transport variable $\tilde{Re}_{\theta t}$ can convect from the stagnation point through the boundary layer and diffuse from the free stream into the boundary layer.

The transport equation for the intermittency $\gamma$ is used by Langtry and Menter (2009) to model natural and bypass transition. The production term $P_\gamma$ in Eq. (10) above

$$P_\gamma = F_\mathrm{length}\cdot c_{a1}\cdot\rho\cdot S\cdot[\gamma\cdot F_\mathrm{onset}]^{0,5}\cdot(1-c_{e1}\cdot\gamma) \tag{13}$$

includes factors for the length $F_\mathrm{length}$ and the onset point of the transition $F_\mathrm{onset}$. The function of $F_\mathrm{length}$ is defined by a correlation of the transported scalar $\tilde{Re}_{\theta t}$ and a modification term $F_\mathrm{sublayer}$ which are described by Langtry and Menter (2009). The modification term $F_\mathrm{sublayer}$ includes the specific dissipation rate $\omega$ and is designed to prevent a non-physical increase in the skin friction. The function of $F_\mathrm{onset}$ is based on the following

equations

$$F_{\text{onset}} = \max(F_{\text{onset2}} - F_{\text{onset3}}, 0),$$

$$F_{\text{onset2}} = \min(\max(F_{\text{onset1}}, F_{\text{onset1}}^4), 2.0), \tag{14}$$

$$F_{\text{onset1}} = \frac{Re_V}{2.193 Re_{\theta c}},\ F_{\text{onset3}} = \max\left(1 - \left(\frac{R_{\text{T}}}{2.5}\right)^3, 0\right)$$

with the vorticity Reynolds number $Re_V$, the critical Reynolds number $Re_{\theta c}$, and the eddy-viscosity ratio $R_{\text{T}}$:

$$Re_V = \frac{\rho y^2 S}{\mu},\ Re_{\theta c} = f(\tilde{Re}_{\theta t}),\ R_{\text{T}} = \frac{\mu_{\text{T}}}{\mu}. \tag{15}$$

As could be derived from the full set of equations, the modification of the specific dissipation rate $\omega$ by the turbulence model for rough walls (cf. Eq. 8 and 9) must have an effect via the increased eddy viscosity ratio $R_{\text{T}}$ of the function $F_{\text{onset3}}$ (cf. Eq. 14 and 15) on the roughness-induced transition prediction due to an increased production of $\gamma$ (cf. Eq. 13).

Dassler et al. (2012) developed an extension for the $\gamma$-$Re_\theta$ transition model to explicitly consider the rough-wall boundary condition in the transition model. A third transport equation for the non-dimensional value $A_r$

$$\frac{D(\rho A_r)}{Dt} = \frac{\partial}{\partial x_j}\left[\sigma_{A_r}(\mu + \mu_{\text{T}})\frac{\partial A_r}{\partial x_j}\right] \tag{16}$$

is added to the model. Similar to the incorporation of a rough-wall boundary condition in the $\omega$-equation of the turbulence model, the value of $A_r$ is correlated with the local non-dimensional sand-grain roughness $k_{\text{s}}^+$

$$A_{r,W} = 8 \cdot k_{\text{s}}^+ \tag{17}$$

at the wall. This allows to convect and diffuse the roughness effect into the flow field. By a variable $Arg_r$ the production term $P_{\theta t}$ of $\tilde{Re}_{\theta t}$ is modified as follows:

$$P_{\theta t} = c_{\theta t}\frac{\rho}{t}\left[\left(Re_{\theta t} - \tilde{Re}_{\theta t}\right)(1 - F_{\theta t}) - Arg_r\right]. \tag{18}$$

The variable $Arg_r$ is a function of the transported value $A_r$ and adds sensitivity to the momentum thickness Reynolds number $\tilde{Re}_{\theta t}$. To conclude, a reduction of the transport value $\tilde{Re}_{\theta t}$ by surface roughness is obtained via the rough-wall boundary condition. This results in a shift of the transition to an upstream position.

The coupling of the turbulence and transition models is performed by a multiplication of the locally highest intermittency $\gamma$ with the production and destruction terms of the turbulent kinetic energy of the turbulence model. Thus, the rough-wall boundary condition acting on the turbulence production can already influence the transition model.

## NUMERICAL METHOD

For the CFD simulations, the non-commercial flow solver TRACE 9.1 (Nürnberger, 2004; Franke et al., 2005; Kugeler et al., 2008) from the Institute of Propulsion Technology at the German Aerospace Center (DLR) is used. Based on a finite-volume method with structured multi-block meshes, TRACE solves the three-dimensional Favre-averaged Navier-Stokes equations. To discretize the convective fluxes, the second-order upwind scheme of Roe's is used, while the diffusive fluxes are discretized by a central differencing scheme. A converged solution satisfies a mass-imbalance < 0.1% and an asymptotic convergence of the eddy-viscosity and pressure ratio. This is accompanied by maximum residuals lower than 1e-8.

In the following, different transition and turbulence model combinations implemented in TRACE are analyzed in an annular wind tunnel test case with respect to rough-wall boundary conditions. To assess the current implemented state in roughness-induced transition modeling, the $\gamma$-$Re_\theta$ model with added roughness model is compared to the original $\gamma$-$Re_\theta$ model and experimental results. Both models are combined with the $k$-$\omega$ turbulence model. Next, the sensitivity of transition onset on a rough-wall boundary condition of the SST model in combination with the original $\gamma$-$Re_\theta$ model is analyzed.

## ANNULAR WIND TUNNEL TEST CASE

The RANS-based transition prediction of rough walls is studied with an annular wind tunnel test case published by Feindt (1956). By using different types of emery paper and annular geometries, Feindt measured the effect of different surface roughness heights and linear pressure gradients on the transition onset. The emery paper was applied to the inner cylinder, while the outer cylinder was used to impress the pressure gradients to the flow. The effect of surface roughness on the transition onset without pressure gradient was measured in the free stream. As a result, Feindt stated that the transition onset is affected by surface roughness when $Re_{k_{\text{s}}} > 120$. Dassler (Dassler et al., 2012; Dassler, 2013) simplified the test case to a flat plate and used the results of Feindt to validate the developed roughness extension of the $\gamma$-$Re_\theta$ model.

The numerical domains used in the present study were generated by Alldieck (2019) with the software G3D-Hexa Version 4.95, see Fig. 1. To compare with the experimental measurements, the annular geometries were built with the pressure gradients given by Feindt, see Tab. 1, as follows:

$$r(x) = \sqrt{\frac{r_1^2}{\sqrt{1.0 - \text{PG}}}} \text{ with : PG} = \frac{p_2 - p_1}{p_{\text{tot},1} - p_1}. \tag{19}$$

**Table 1**: Measured pressure gradients by Feindt (1956)

| | zero PG | adverse PG | favorable PG |
|---|---|---|---|
| dp/dx | 0 $m^{-1}$ | 0,371 $m^{-1}$ | -0,487 $m^{-1}$ |

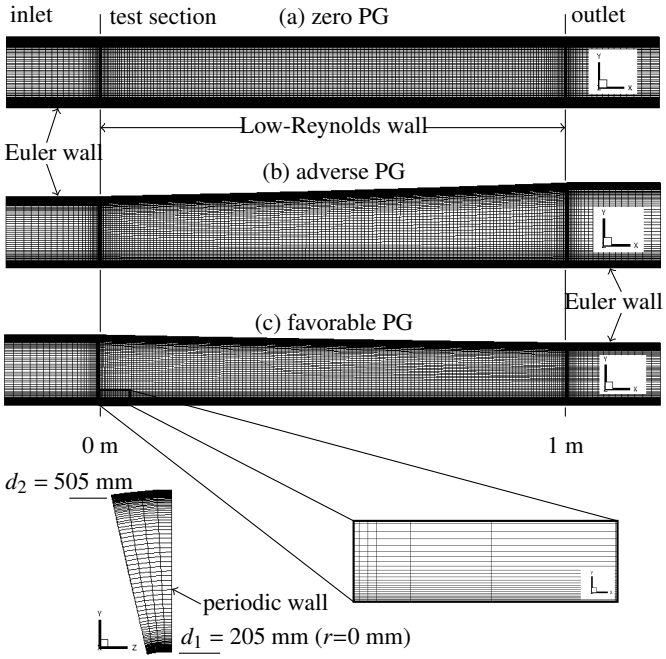


**Figure 1**: Computational grids of Feindt's test cases: zero and linear pressure gradients. Detail view of the tunnel front section and hub wall (Alldieck, 2019).

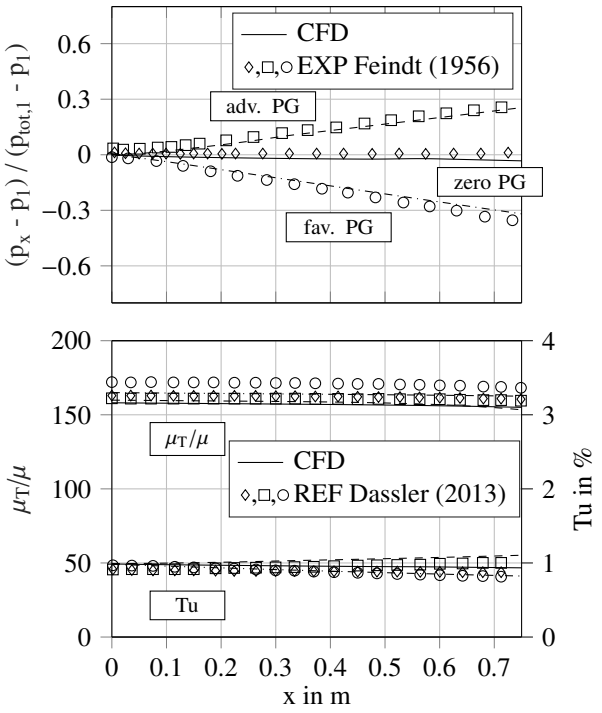


**Figure 2**: Validation of the computational domains at a hub wall distance of $r$ = 25 mm (Alldieck, 2019).

To achieve a high grid resolution in the boundary layer, the first node to wall distance was set to $y^+ \ll 1$ with a grid growth rate of 1.1. The generated meshes consist of approximately 114,000 cells. A grid refinement study according to Roache (1994) showed a Grid Convergence Index (GCI) for the integral pressure gradient of GCI=0.007%. All numerical domains consist of three blocks. The in- and outlet block are set to the Euler wall condition for simulating the in- and outflow of the annular wind tunnel and adjusting the turbulent decay in the inflow. The test section is set to one pitch periodic with an angle of 11.25° and 4 cells in circumferential direction. At the inner and outer cylinder, a viscous wall condition is used. A high grid resolution near the stagnation point is needed to prevent a non-physical production of turbulent kinetic energy.

A free stream velocity at the inlet of the test section of approximately $U_1 = 20\ \frac{\mathrm{m}}{\mathrm{s}}$ was set by using a total inlet pressure of $p_{\mathrm{tot},1}$ = 101565 Pa. Correspondingly, the total inlet temperature was set to $T_{\mathrm{tot},1} = 293{,}349$ K. Using this setup, the pressure gradients reported by Feindt (1956) could be well predicted, see Fig. 2. Only for the zero pressure gradient flow a slight acceleration shows compared with the experiment. This is caused by the boundary layer at the outer cylinder, which was not present in the experiments due to the measurements in the free stream. However, the slight acceleration is also evident in the flat plate test case of Dassler et al. (2012).

In the experiments, Feindt (1956) measured a turbulence intensity in the free stream of the test section of approximately Tu ~ 1%. In order to predict the transition onset for a smooth surface with the $\gamma$-$Re_\theta$ model, the turbulent length scale was iterated to be $L_t = 0{,}01$ m, compare Fig. 5 (Bode et al., 2014). As can be seen in Fig. 2, the turbulence intensity Tu and the eddy-viscosity ratio $\mu_T/\mu$ correlate with the data presented by Dassler (2013).

## RESULTS AND DISCUSSION

### Validation

Four different sand-grain roughness heights according to the measurements described by Feindt (1956) have been used in the numerical study. Table 2 provides the applied sand-grain values $k_s$ and the corresponding equivalent sand-grain roughness Reynolds number $Re_{k_s}$

$$Re_{k_s} = \frac{k_s U_1}{\nu} \tag{20}$$

calculated with the kinematic viscosity $\nu = 15.06 \times 10^{-6}\,\frac{\mathrm{m}^2}{\mathrm{s}}$.

First, the resulting friction coefficients for the different transition and turbulence model combinations are analyzed. The curves of the friction coefficient contain information about the modeled transition onset and effect of surface roughness. Figure 3 shows the simulation results of the $k$-$\omega$ model in combination with the $\gamma$-$Re_\theta$ model for both, original model, and activated roughness model (RM). As expected, the transition onset is moving downstream when decreasing the pressure

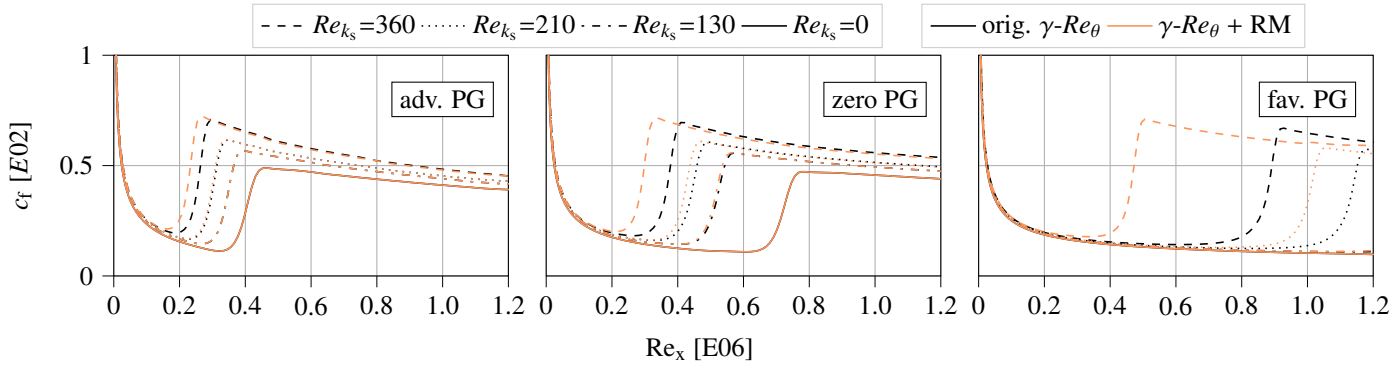


**Figure 3**: Roughness-based friction coefficient for the combination of $\gamma$-$Re_\theta$ and $k$-$\omega$ with different pressure gradients. The original $\gamma$-$Re_\theta$-model is represented by the black lines. The orange lines indicate the $\gamma$-$Re_\theta$-model with roughness modification. Especially for small $Re_{k_s}$ the lines of both models overlap.

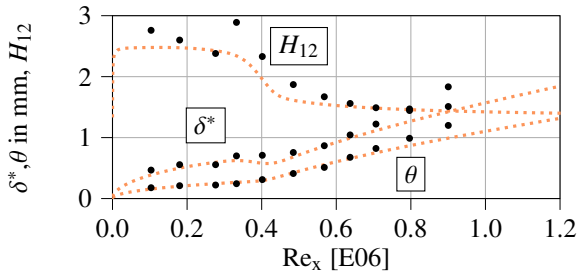


**Figure 4**: Comparison of displacement and momentum thickness for $Re_{k_s}$ = 210 between RM prediction and experiment with zero pressure gradient.

gradient. In contrast, the transition moves upstream with increased surface roughness. This effect is bigger with favorable than adverse pressure gradients. However, the effect of surface roughness on the transition onset already shows for the original $\gamma$-$Re_\theta$ model without roughness extension. Depending on the $Re_{k_s}$, the roughness extension predicts a further shift of the transition onset. For low $Re_{k_s}$~120, this effect is quite small but increases with higher $Re_{k_s}$. In addition, the shift of the transition onset modeled by the roughness extension depends on the pressure gradient. Figure 4 presents a detailed comparison of the displacement and momentum thickness development of zero pressure gradient with a roughness of $Re_{k_s}$ = 210 between the numerical simulation and experiment. The experimental

**Table 2**: Investigated equivalent sand roughness by Feindt (1956)

| | 1 | 2 | 3 | 4 |
|---|---|---|---|---|
| $k_s$ in $\mu$m | 0 | 100 | 160 | 280 |
| $Re_{k_s}$ | 0 | 130 | 210 | 360 |

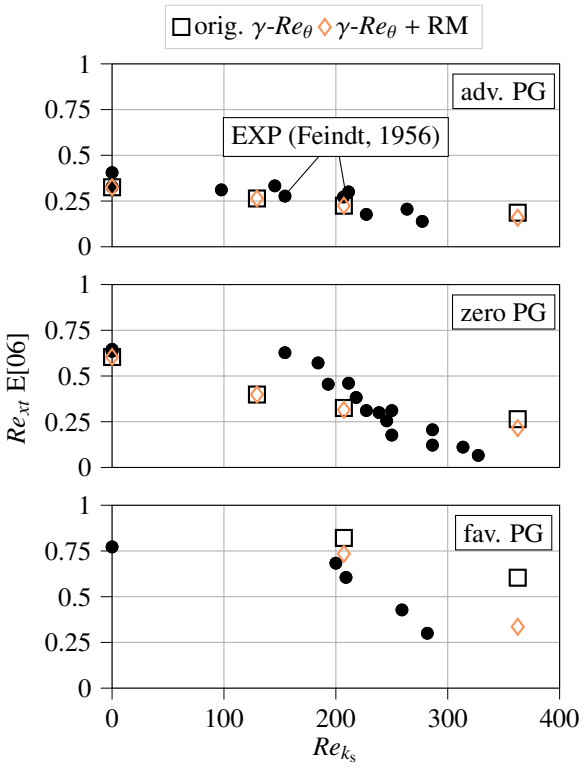


**Figure 5**: Transition onset $Re_{xt}$ dependency on critical roughness Reynolds-number $Re_{k_s}$ for different pressure gradients.

results are well predicted by the $\gamma$-$Re_\theta$ model with activated roughness extension in the laminar and transitional boundary layer. Only in the turbulent boundary layer, a difference between the prediction and experimental results occurs due to the decelerated flow of the experiments at the end of the test section. Figure 5 gives a detailed view of the correlation between the surface roughness height and transition onset. Here, the transition onset $Re_{xt}$ is plotted as a function of the surface

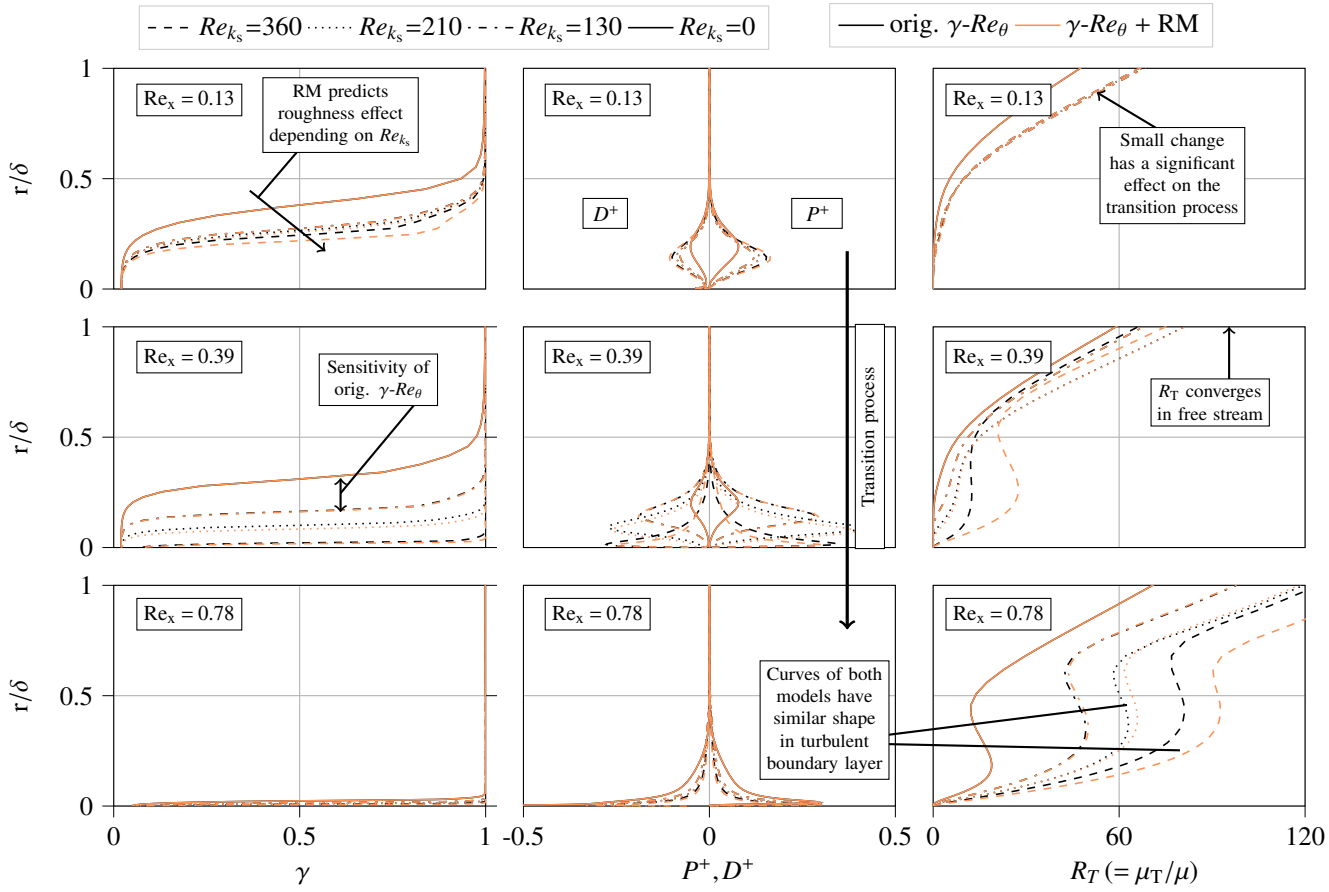


**Figure 6**: Roughness-based intermittency $\gamma$, turbulent kinetic energy production $P^+$ and dissipation $D^+$, and eddy-viscosity ratio $\mu_T/\mu$ with zero pressure gradient at three different positions for $\gamma$-$Re_\theta$ – $k$-$\omega$ . The original $\gamma$-$Re_\theta$-model is represented by the black lines. The orange lines indicate the $\gamma$-$Re_\theta$-model with roughness modification. The state of the boundary layer triggered by the plotted quantities strongly depends on the roughness height.

roughness height $Re_{k_s}$and pressure gradient. Additionally, the measurements of Feindt (1956) are plotted. As Dassler et al. (2012) proposed, the transition onset $\mathrm{Re}_{xt}$ is defined by the minimum of the friction coefficient $c_f$. This point agrees with the definition of Feindt (1956). At this location, the shape factor starts to abruptly decrease, because the relation of the displacement and momentum thickness changes. Referring back to Fig. 4, this change can be seen in both, the numerical results and experiments. The aforementioned accurate prediction of the transition onset for $Re_{k_s}$=210 with zero pressure gradient is also evident in Fig. 5. In addition, the transition onset of a smooth wall is well predicted by the $\gamma$-$Re_\theta$ model with both, adverse and zero pressure gradient. For a smooth wall and small surface roughness heights, no transition occurs along the test section with a favorable pressure gradient. However, as apparent in the figure, the transition onset modeled with the activated roughness model shows deficits when reproducing the experiments. As reported by Feindt (1956), surface roughness has no effect on the transition onset for $Re_{k_s} < 120$. In contrast to the validation of the roughness model with a flat plate by Dassler et al. (2012), this finding is not confirmed by the simulation in this work. Based on the sensitivity of the original $\gamma$-$Re_\theta$ model to surface roughness, it can be inferred that there is a disturbing effect of the turbulence model on the transition modeling induced by the rough-wall boundary condition.

## Model Analysis

To analyze the sensitivity of the original $\gamma$-$Re_\theta$ model to surface roughness in more detail, this section turns to the interaction of the turbulence and transition model. Figure 6 presents the intermittency $\gamma$, the non-dimensional turbulent kinetic energy production $P^+(=\nu P/u_\tau^4)$ and dissipation $D^+(=\nu D/u_\tau^4)$, and the eddy viscosity ratio $\mu_T/\mu$ in the boundary layer at three different positions for zero pressure gradient. As can be seen, $\gamma$ is the driving force to induce the transition. With increased $\gamma$, higher $P^+$, $D^+$, and $\mu_T/\mu$ are evident. Surface roughness accelerates this process, even if the roughness model of the transition model is deactivated. Thus, there is a significant effect of the rough-wall boundary condition modeled by the turbulence model on the transition model. To assess the iso-

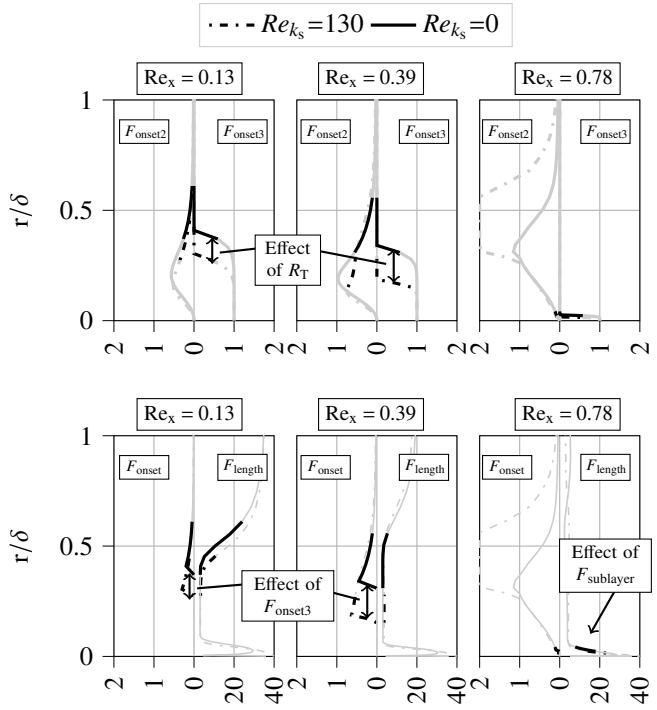


**Figure 7**: Roughness-based intermittency production functions $F_{\text{onset2}}$, and $F_{\text{onset3}}$ in the upper and $F_{\text{length}}$, and $F_{\text{onset}}$ in the lower plots with zero pressure gradient at three different positions for the original $\gamma$-$Re_\theta$ model. (Gray indicates regions with disabled production of $\gamma$)

lated interaction of the roughness model with the turbulence model, the sensitivity of the original $\gamma$-$Re_\theta$ to surface roughness must be eliminated first. In the fully-turbulent boundary layer (Re$_x$ = 0.78), the curves for $\gamma$, $P^+$, $D^+$, and $\mu_T/\mu$ of both transition models adapt to each other and show identical shapes. This, in turn, is caused by the rough-wall correlation of the $k$-$\omega$ formulation and is modeled independently from the transition model.

To explain the sensitivity of the original $\gamma$-$Re_\theta$ model on the rough-wall modeling of the $k$-$\omega$ formulation, the functions $F_{\text{onset}}$ and $F_{\text{length}}$ of the intermittency production are taken into account and are illustrated in Fig. 7. The figure shows the development of both factors with zero pressure gradient for a smooth wall and low $Re_{k_s}$=130. The production of $\gamma$ is zero if $\gamma = 1$ or $F_{\text{onset}} = 0$. These parts are plotted in gray, whereas parts with active production are plotted in black. The function $F_{\text{onset}}$ takes higher values for the rough than smooth surface. In contrast, the difference in $F_{\text{length}}$ is quite small. Dassler (2013) reported that the function $F_{\text{sublayer}}$ which modifies $F_{\text{length}}$ causes the shift of transition onset to an upstream position for a rough wall. Here, it shows that the effect of $F_{\text{sublayer}}$ including the dissipation rate $\omega$ first occurs towards the end of transition. More significant is $F_{\text{onset}}$, which is calculated with the critical Reynolds number via $F_{\text{onset2}}$ and eddy-viscosity ratio via $F_{\text{onset3}}$. A comparison

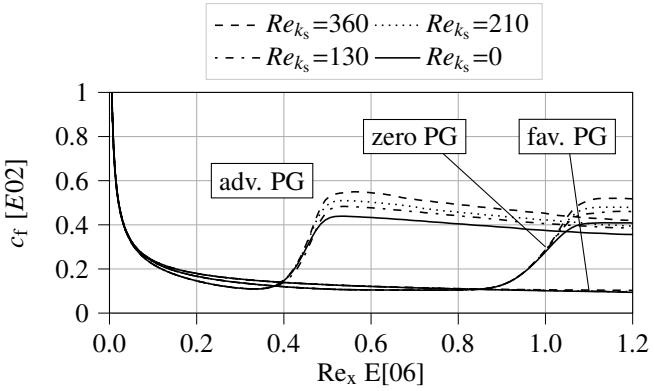


**Figure 8**: Roughness-based friction coefficient of original $\gamma$-$Re_\theta$ in combination with SST for different pressure gradients.

of both functions $F_{\text{onset2}}$ and $F_{\text{onset3}}$ shows that $F_{\text{onset3}}$ is more sensitive to surface roughness. This is caused by the higher eddy-viscosity ratio $\mu_T/\mu$ which increases for rough surfaces, see last column in Fig. 6. Consequently, the transition is forced by the turbulence modeling of the rough wall increasing $\mu_T/\mu$ and $F_{\text{onset}}$, respectively. The length of the transition is negligible affected by the wall boundary condition in the turbulence model.

### SST Approach

In order to identify the reason behind the sensitivity of the original $\gamma$-$Re_\theta$ model on the rough-wall boundary condition, the interaction of the $\gamma$-$Re_\theta$ – SST model obtained is analyzed. Figure 8 shows the friction coefficients using the SST model. The adverse pressure gradient boundary layer is the first to turn from laminar to turbulent, followed by zero pressure gradient. Like the $k$-$\omega$ model, the SST model predicts no transition with favorable pressure gradient flow. Surprisingly, the effect of surface roughness modeled on the transition by the rough-wall boundary condition in the turbulence model is quite small in all cases. The increased frictional losses are only visible in the turbulent boundary layer.

Figure 9 and 10 focus on the interaction of the original $\gamma$-$Re_\theta$ model combined with the SST model for zero pressure gradient. As evident in Fig. 9, a rough wall has no effect on the intermittency. This results in an identical production and destruction of turbulent kinetic energy compared to a smooth surface. This, in turn, is followed by an identical eddy-viscosity ratio between rough and smooth surfaces. One reason could be the Bradshaw assumption of the SST model which limits the rough-wall condition in the $k$-$\omega$ formulation, as shown by Hellsten and Laine (1997). Accordingly, Figure 9 shows the quotient of the Bradshaw assumption and the original $k$-$\omega$ formulation for the eddy-viscosity. A value below one indicates that the $k$-$\omega$ formulation is used and a value above one corresponds to the Bradshaw assumption. Thus, the $k$-$\omega$ formulation

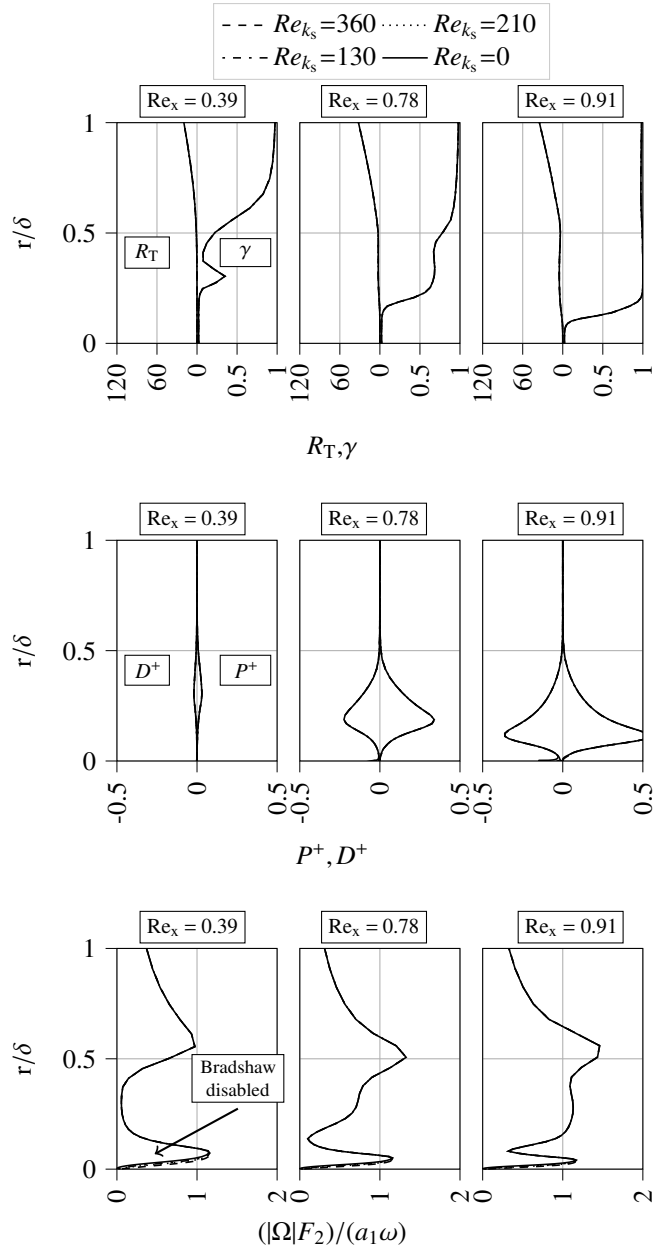


**Figure 9**: The eddy-viscosity ratio $R_T$, intermittency $\gamma$, non-dimensional turbulence-energy production $P^+$ and dissipation $D^+$, and ratio $(|\Omega|F_2)/(a_1\omega)$ at three different positions and zero pressure gradient for $\gamma$-$Re_\theta$ – SST .

is present in the laminar flow. Consequently, no limitation depending on the turbulence model on the rough-wall boundary condition is expected. Subsequently, the advantageous effect of the SST model on the transition modeling of rough-wall boundary condition must be caused by the added cross-diffusion term and reduced free stream sensitivity. However, the robustness of the eddy-viscosity ratio against surface roughness affects the transition functions $F_{\text{onset}}$ and $F_{\text{onset3}}$. As presented in Figure

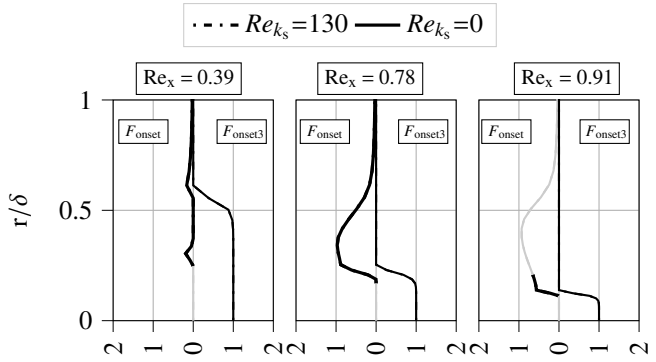


**Figure 10**: Roughness-based transition model function $F_{\text{onset}}$ and $F_{\text{onset3}}$ with zero pressure gradient at three different positions for $\gamma$-$Re_\theta$ – SST . (Gray indicates regions with disabled production of $\gamma$)

10, $F_{\text{onset3}}$ shows no sensitivity to surface roughness. Similar to Fig. 7, the bold lines for $F_{\text{onset}}$ indicate that the production of $\gamma$ is activated. Referring back to the fundamentals, the eddy-viscosity ratio $R_T$ modifies the term of $F_{\text{onset}}$ via the function of $F_{\text{onset3}}$. To conclude, the effect of the rough-wall boundary condition on the transition process is damped by the SST model.

In summary, adding a third transport equation is a good approach which incorporates rough-wall boundary conditions in transition modeling. Nevertheless, the transition prediction is significantly affected by the effect of rough-wall boundary condition in the turbulence model. This leads to imprecise predictions of roughness-induced transition onset in combination with the $k$-$\omega$ model. As shown in combination with the SST model, a higher robustness of the eddy-viscosity ratio against surface roughness can disable the effect of the turbulence model on the transition model in the laminar boundary layer when modeling rough-wall boundary conditions. However, the SST model reveals deficits in turbulent rough wall boundary layer flows (Hellsten and Laine, 1997).

## CONCLUSIONS

In the present study, transition modeling of a rough-wall boundary condition using RANS-based model formulations was validated with an annular wind tunnel test case. The predictive quality of the transition model was explored under different pressure gradients and for various surface roughness heights of the experimental data set.

A comparison of different transition and turbulence model combinations shows a wide range of predicted transition mechanism and locations. None of the investigated model combinations were able to predict the point of transition for various roughness heights under different pressure gradients. This behavior is due to the interaction of the turbulence model with the transition model. In summary, the following conclusions can be drawn:

1. Rough-wall simulations conducted with the original $\gamma$-$Re_\theta$ model reveal a large effect of the turbulence model on the transition location triggered via the term $F_{\text{onset}}$.
2. Caused by the robustness of the eddy-viscosity ratio against surface roughness in the SST model, no sensitivity of the transition onset on surface roughness shows for the original $\gamma$-$Re_\theta$ model.
3. Using a third transport equation to incorporate rough-wall boundary condition in the $\gamma$-$Re_\theta$ model has been confirmed as a good approach. So far, the transition onset was not precisely predicted not least due to the aforementioned interaction of the turbulence model with the transition model.

Therefore, further work in roughness-induced transition modeling should focus on eliminating the effect of the rough-wall boundary condition in the turbulence model on the transition model. Regarding the $\gamma$-$Re_\theta$ model, the effect of limiting the eddy-viscosity ratio in the function $F_{\text{onset}}$ should be studied. Accordingly, the robustness of roughness-induced transition modeling against the turbulence model used would be increased.

## NOMENCLATURE

$c_\text{f}$ friction coefficient
$D^+ = \frac{\nu D}{u_\tau^4}$ non-dimensional turbulent kinetic energy destruction
$F_{\text{length}}$ function of transition length
$F_{\text{onset}}$ function of transition onset
$H_{12}$ shape factor
$k$ turbulent kinetic energy
$K$ acceleration parameter
$k_\text{s}$ equivalent sand-grain roughness
$k_\text{s}^+$ non-dimensional equivalent sand-grain roughness
$L_\text{t}$ turbulent length scale
$P^+ = \frac{\nu P}{u_\tau^4}$ non-dimensional turbulent kinetic energy production
$p$ static pressure
$p_\text{tot}$ total pressure
$R_\text{T}$ eddy-viscosity ratio
Re Reynolds number
$\text{Re}_\text{x}$ local Reynolds number
$Re_V$ vorticity Reynolds number
$Re_\theta$ momentum-thickness Reynolds number
$Re_{\theta t}$ transition onset momentum-thickness Reynolds number
$\tilde{Re}_{\theta t}$ local transition onset momentum-thickness Reynolds number
$Re_{\theta c}$ critical momentum-thickness Reynolds number
S strain-rate
$T_\text{tot}$ total temperature
Tu turbulence intensity
$U$ velocity magnitude
$u_{i,j}$ velocity
$u_\tau$ wall shear stress velocity
$x_{i,j}$ position
$\gamma$ intermittency
$\delta$ thickness boundary layer
$\delta^*$ displacement thickness
$\theta$ momentum thickness
$\lambda_\theta$ pressure gradient parameter
$\mu$ dynamic molecular viscosity
$\mu_\text{T}$ eddy viscosity
$\nu$ kinematic molecular viscosity
$\rho$ density
$\tau_{ij}$ shear stress
$\tau_\text{W}$ wall shear stress
$\omega_{\text{rough}}$ rough wall turbulent dissipation
$\omega$ specific dissipation rate
$\Omega$ vorticity
CFD Computational Fluid Dynamics
DLR German Aerospace Center
EXP Experiment
GCI Grid Convergence Index
PG Pressure Gradient
RANS Reynolds-Averaged Navier-Stokes
REF Reference
RM Roughness Model
SST Shear Stress Transport
TRACE Turbomachinery Research Aerospace Computational Environment

## ORCID ID


Robert Alldieck orcid.org/0000-0001-9621-3120
Hendrik Seehausen orcid.org/0000-0001-9959-8468
Florian Herbst orcid.org/0000-0003-0993-4582
Joerg R. Seume orcid.org/0000-0003-2007-7905


## ACKNOWLEDGMENTS


The present work has been carried out in the subproject B3 within the Collaborative Research Center (CRC) 871 "Regeneration of Complex Capital Goods" which is funded by the Deutsche Forschungsgemeinschaft (DFG, German Research Foundation) – SFB 871/3 – 119193472. The authors would like to thank the DFG for the support. Moreover, the authors would like to acknowledge the substantial contribution of the DLR Institute of Propulsion Technology and MTU Aero Engines AG for providing TRACE.


## REFERENCES


Abu-Ghannam, B. and Shaw, R. (1980). Natural transition of boundary layers—the effects of turbulence, pressure gradient, and flow history. *Journal of Mechanical Engineering Science*, 22(5):213–228.

Alldieck, R. (2019). *Numerische Untersuchung über die Wiedergabegenauigkeit der rauheitsinduzierten Transition bestehender Transitionsmodelle*. Master thesis, Leibniz Universität Hannover, Hannover.

Bode, C., Aufderheide, T., Kožulović, D., and Friedrichs, J. (2014). The effects of turbulence length scale on turbulence and transition prediction in turbomachinery flows. volume

Volume 2B: Turbomachinery of *Turbo Expo: Power for Land, Sea, and Air*.

Bons, J. P. (2010). A review of surface roughness effects in gas turbines. *ASME J. Turbomach.*, 132(2):021004.

Boyle, R. J. and Senyitko, R. G. (2003). Measurements and predictions of surface roughness effects on the turbine vane aerodynamics. volume Volume 6: Turbo Expo 2003, Parts A and B of *Turbo Expo: Power for Land, Sea, and Air*, pages 291–303.

Dassler, P. (2013). *Modellierung der Grenzschichttransition auf rauen Oberflächen in Turbinen*. Phd thesis, Technische Universität Braunschweig, Braunschweig.

Dassler, P., Kožulović, D., and Fiala, A. (2012). Transport equation for roughness effects on laminar–turbulent transition. Conference on Modelling Fluid Flow (CMFF '12), Budapest, Hungary.

Feindt, E. G. (1956). *Untersuchungen über die Abhängigkeit des Umschlages laminar-turbulent von der Oberflächenrauhigkeit und der Druckverteilung*. PhD thesis.

Franke, M., Kuegeler, E., and Nürnberger, D. (2005). Das dlr-verfahren trace: Moderne simulationstechniken für turbomaschinenströmungen. In *DGLR Congress*.

Gilge, P., Hohenstein, S., and Seume, J. (2017). Experimental investigation of the aerodynamic effect of local surface roughness on a turbine blade. *International Journal of Gas Turbine*, 9:12.

Hellsten, A. and Laine, S. (1997). Extension of the k-omega-sst turbulence model for flows over rough surfaces. *22nd Atmospheric Flight Mechanics Conference*.

Herbst, F., Fiala, A., and Seume, J. R. (2014). Modeling Vortex Generating Jet-Induced Transition in Low-Pressure Turbines. *Journal of Turbomachinery*, 136(7).

Hohenstein, S., Aschenbruck, J., and Seume, J. (2013a). Aerodynamic effects of non-uniform surface roughness on a turbine blade. volume Volume 6A: Turbomachinery of *Turbo Expo: Power for Land, Sea, and Air*.

Hohenstein, S., Gilge, P., Raulf, C., and Seume, J. (2013b). Einfluss lokaler rauheiten auf die aerodynamischen verluste von turbinenschaufeln. Beitrag auf dem Deutschen Luft- und Raumhfahrtkongress.

Hummel, F., Lötzerich, M., Cardamone, P., and Fottner, L. (2005). Surface Roughness Effects on Turbine Blade Aerodynamics. *Journal of Turbomachinery*, 127(3):453–461.

Koepplin, V., Herbst, F., and Seume, J. R. (2017). Correlation-Based Riblet Model for Turbomachinery Applications. *Journal of Turbomachinery*, 139(7).

Kožulović, D. (2007). *Modellierung des Grenzschichtumschlages bei Turbomaschinenströmungen unter Berücksichtigung mehrerer Umschlagsarten*. Phd thesis, Ruhr-Universität Bochum, Bochum.

Kugeler, E., Nurnberger, D., Weber, A., and Engel, K. (2008). Influence of blade fillets on the performance of a 15 stage gas turbine compressor. In *ASME Turbo Expo 2008: Power for Land, Sea, and Air*, pages 415–424. American Society of Mechanical Engineers.

Langtry, R. B. and Menter, F. R. (2009). Correlation-based transition modeling for unstructured parallelized computational fluid dynamics codes. *AIAA Journal*, 47(12):2894–2906.

Mayle, R. E. (1991). The 1991 igti scholar lecture: The role of laminar-turbulent transition in gas turbine engines. *ASME J. Turbomach.*, 113(4):509–536.

Menter, F., Smirnov, P., Liu, T., and Avancha, R. (2015). A one-equation local correlation-based transition model. *Flow, Turbulence and Combustion*, 95:1–37.

Menter, F. R. (1994). Two-equation eddy-viscosity turbulence models for engineering applications. *AIAA Journal*, 32(8):1598–1605.

Menter, F. R., Langtry, R. B., Likki, S. R., Suzen, Y. B., Huang, P. G., and Völker, S. (2006). A correlation-based transition model using local variables—part i: Model formulation. *Journal of Turbomachinery*, 128(3):413.

Müller, C. and Herbst, F. (2014). Modelling of crossflow-induced transition based on local variables. In Proc. ECCOMAS, Paper No. 2252, Barcelona (Spain).

Nikuradse, J. (1933). *Strömungsgesetze in rauhen Rohren*. Forschungsheft auf dem Gebiete des Ingenieurwesens. VDI-Verlag.

Nürnberger, D. (2004). *Implizite Zeitintegration für die Simulation von Turbomaschinenströmungen*. PhD thesis, Ruhr-Universität Bochum.

Roache, P. J. (1994). Perspective: A method for uniform reporting of grid refinement studies. *Journal of Fluids Engineering*, 116(3):405–413.

Schlichting, H. (1936). Experimentelle untersuchungen zum rauhigkeitsproblem. *Ingenieur-Archiv*, 7(1):1–34.

Stripf, M., Schulz, A., and Bauer, H. (2008). Modeling of rough-wall boundary layer transition and heat transfer on turbine airfoils. *ASME J. Turbomach.*, 130(2):021003.

Stripf, M., Schulz, A., and Wittig, S. (2005). Surface Roughness Effects on External Heat Transfer of a HP Turbine Vane . *Journal of Turbomachinery*, 127(1):200–208.

Suzen, Y. B., Xiong, G., and Huang, P. G. (2002). Predictions of transitional flows in low-pressure turbines using intermittency transport equation. *AIAA Journal*, 40(2):254–266.

Walters, D. and Cokljat, D. (2008). A three-equation eddy-viscosity model for reynolds-averaged navier–stokes simulations of transitional flow. *Journal of Fluids Engineering*, 130(12).

Walters, D. K. and Leylek, J. H. (2004). A New Model for Boundary Layer Transition Using a Single-Point RANS Approach . *Journal of Turbomachinery*, 126(1):193–202.

Wilcox, D. C. (1988). Reassessment of the scale-determining equation for advanced turbulence models. *AIAA Journal*, 26(11):1299–1310.